An experimental vibration-buckling investigation on classical and variable angle tow composite shells under axial compression

Labans, E.; Abramovich, H.; Bisagni, C.

DOI
10.1016/j.jsv.2019.02.034

Publication date
2019

Document Version
Final published version

Published in
Journal of Sound and Vibration

Journal of Sound and Vibration 449 (2019) 315–329

Contents lists available at ScienceDirect

Journal of Sound and Vibration

journal homepage: www.elsevier.com/locate/jsvi

An experimental vibration-buckling investigation on classical and variable angle tow composite shells under axial compression

E. Labans [a], H. Abramovich [b,*], C. Bisagni [a]

[a] Aerospace Structures and Computational Mechanics, Faculty of Aerospace Engineering, Delft University of Technology, 2629 HS, Delft, the Netherlands
[b] Faculty of Aerospace Engineering, Technion, I.I.T., 32000, Haifa, Israel

ARTICLE INFO

Article history:
Received 27 June 2018
Received in revised form 31 January 2019
Accepted 24 February 2019
Available online 4 March 2019
Handling Editor: S. Ilanko

Keywords:
Natural frequency
Axial compression
Composite cylindrical shell
Vibration Correlation Technique

ABSTRACT

Two laminated composite shells, one with a conventional straight fiber laminate denoted the classical laminated shell and the second one with a variable angle tow reinforced composite, had been excited and their natural frequencies and mode shapes had been measured and monitored as a function of the axial compression load. Then, the in-situ buckling loads of the two tested specimens were predicted using the Vibration Correlation Technique (VCT) and compared with actual experimental buckling loads and Finite Element buckling predictions, yielding matching, consistent and repeatable results. It was shown that the VCT predicts the actual in-situ buckling loads of laminated composite thin walled cylindrical shells with a high accuracy, yielding 96% and 98.6% of the experimental buckling load, for the classical and variable angle tow composite shells, respectively. These results, although based on only two specimens, join the relatively small data base published in the literature, proving the nondestructive nature of the VCT approach, making it an adequate method for application on thin-walled structures, like shells. In addition, some testing recommendations are presented, to effectively enable the successful application of the VCT for in-situ buckling prediction of the buckling sensitive structures, like composite cylindrical shells.

1. Introduction

Thin walled structures, like shells loaded in compression, are susceptible to initial geometric imperfections, boundary conditions and load eccentricity. This leads to a large scatter between the numerical prediction of the buckling loads and their experimental counterparts. To enable a safe use of shell structures, NASA had issued a series of monographs [1–4] for various types of shells and their applied loadings, aimed at providing designers with reliable tools for shell type constructions. However, those tools provide reduction factors, known as knock-down factors by which the numerical buckling load should be multiplied to yield the designed buckling load. These factors depend on the type of the loading, shape of the shell and the radius/thickness, and might reach down to 25% of the calculated load, that for some shells lead to conservative design. This led to a relatively new NASA project, the *SBKF* (*S*hell *B*uckling *Knockdown F*actor) aimed at developing less-conservative robust

* Corresponding author.
E-mail address: haim@technion.ac.il (H. Abramovich).

https://doi.org/10.1016/j.jsv.2019.02.034

shell buckling design factors for launch vehicles. It also enables the reduction of their mass and increasing performance, reliability, robustness and increased payload capability [4]. In parallel, European projects were also conducted, like *DAEDALOS* (*D*ynamics in *A*ircraft *E*ngineering *D*esign and *A*nalysis for *L*ight *O*ptimized *S*tructures) [5–7] and *DESICOS* (New Robust *Desi*gn Guideline for Imperfection Sensitive *Co*mposite Launcher *S*tructures) [8].

One of the effective ways, to contribute to the reduction of the above stated scatter, is to use a nondestructive predictor for the in-situ experimental buckling load of thin walled structures, like cylindrical shells. It should be stressed that a true nondestructive method, viable from the engineering point of view, would predict the in-situ buckling load of the tested structure from "below" the actual buckling load. One of those nondestructive methods is known in the literature as the Vibration Correlation Technique (VCT). It consists of measuring the in-situ natural frequencies of a loaded structure, and monitoring their change, while the applied compressive load is increased. Assuming the vibrational modes are like the buckling ones, it is possible to draw a curve, displaying the natural frequencies squared vs. the applied load. Extrapolating the curve to zero frequency, would yield the predicted buckling load of the tested structure. Singer et al. [9] dedicated a whole chapter in their book to review the VCT approach and its applications. Another book, recently published [10], reports experimental data on the updated use of the VCT approach for composite shells, presenting promising results.

Besides its capability to non-destructively predict the buckling load of thin-walled structures, the approach can also determine the actual in-situ boundary conditions of the structures, and therefore the VCT is usually classified in two main groups according to their application: (a) determination of in-situ boundary conditions, thus yielding a better prediction of the buckling load and (b) direct prediction of the buckling load [11].

Since the early seventies of the previous century, an extensive work had been performed by a group of researchers at the Laboratory of Aeronautical Structures, Faculty of Aerospace Engineering, the Technion, I.I.T., Haifa, Israel, to improve the definition of the in-situ actual boundary conditions of aluminum stringer-stiffened cylindrical shells, loaded in compression leading to a better prediction of their experimental buckling loads [11]. The direct prediction of the buckling loads of compressively loaded shells using the VCT yielded, in most of the cases, loads higher than the experimental ones, and it was shown that, in the vicinity of the buckling load, the curve of frequency squared vs. the compressive load ceases to be linear and performs a sharp bend towards the actual buckling load (zero frequency) due to the inherent initial geometric imperfections of the specimens [12,13]. It is worthwhile to mention that this phenomenon was also found when testing laminated composite curved panels under compressive loads [14]. Therefore, it seemed that the use of the VCT for direct predictions of buckling loads in composite shells was not yet mature enough to be applied in industrial applications, like space launchers. To overcome the above described shortcomings of the method, when applied to thin-walled structures like stiffened cylindrical shells, a new relationship between the natural frequency and the applied compressive load was proposed by Souza et al. [15,16], yielding a better buckling prediction for aluminum stringer-stiffened cylindrical shells, originally tested by the Technion group.

Another approach to improve the applicability of the VCT is a semi-empirical method based on the measurement of the initial geometric imperfections of the shells [17]. Following the approach suggested by Souza et al. [15,16], Arbelo et al. [18,19] and a group from Riga Technical University in Latvia [20–22], proposed a modified empirical VCT approach to predict the experimental buckling load of composite shells, by monitoring the natural frequencies as a function of the applied compressive load. The experimental results presented in Refs. [18–22] show accurate buckling predictions as compared with experimental results, making the modified empirical VCT an applicable tool to predict in-situ buckling of both metal and composite unstiffened shells.

The present manuscript applies the VCT approach on two laminated composite cylindrical shells, one having a classical laminate (straight fiber laminate), while the other having a variable angle tow and compare the VCT predicted results with the experimental and numerical ones, presenting consistent predictions. Both the tests and the numerical analysis have been carried out at the Delft University of Technology.

It is worth mentioning that the variable angle tow idea emerged due to the availability of Automated Fibre Placement (AFP) machines, which enabled researchers to explore advanced ways of enhancing the laminate properties. By placing the fibres in continuous variable angles along the laminate, its properties can be tailored according the given loading, leading to variable-stiffness laminates possessing substantial structural improvements in strength, stiffness and buckling loads. Gurdal et al. [23] and Weaver at al [24–28]. investigated in depth the variable angle tow approach leading to optimization of the laminate layup, and thus yielding thin walled structures, like cylindrical shells, having enhanced structural properties. Therefore, stiffness tailoring of variable angle tow manufactured shells might substantially improve their buckling resistance, thus yielding a more effective structure.

2. The Vibration Correlation Technique (VCT)

The VCT approach, consists of monitoring the variation of the natural frequency while applying axial force. It can be experimentally observed that the application of a compressive load on a thin walled structure reduces its natural frequency. Therefore, by linking the behavior of the natural frequencies and the applied load, one can predict the buckling load of the structure. This can be done in a nondestructive way, by compressing the shell well below the calculated buckling load, constructing a curve of frequency vs. axial compression and then extrapolating the curve to zero frequency, yielding the actual buckling load of the tested specimen.

The application of the VCT to predict the buckling loads of stiffened cylindrical shells in a nondestructive manner, as proposed by Souza et al. [15,16], involves the use of a non-dimensional expression relating the experimental natural frequency and the axial compressive loading written as:

$$(1-p)^2 + \left(1-\xi^2\right)\left(1-f^4\right) = 1 \tag{1}$$

where $p = P/P_{cr}$, $f = \bar{f}/f_0$, P and $\bar{f}$ are the experimentally measured axial compression load and the natural frequency, respectively, f_0 being the natural frequency of the unloaded shell and P_{cr} is defined as the buckling load of the perfect shell. The expression ξ^2, presented in Eq. (1), is defined as the drop in the shell load carrying capacity, squared, based on the experimental results of the performed test, at a relatively low load. This drop can be attributed to the initial geometric imperfections of the tested shell and/or the actual boundary conditions of the tested specimen. The determination of ξ^2 is schematically presented in Fig. 1a.

The measured natural frequency is normalized by the value at zero axial compression, and the axial compression load is also normalized by the calculated buckling load. Then a graph is constructed for $(1-p)^2$ vs. $(1-f^4)$. A linear curve is best fitted among the experimental points. The linear curve would intersect the line $(1-f^4)=1$ at $(1-p)^2 = \xi^2$, as graphically being displayed in Fig. 1a. The predicted buckling load for the tested shell, is then calculated using the following expression:

$$P_{pred.} = (1-\xi)P_{cr} \tag{2}$$

Arbelo et al. [18,19]suggested a modified empirical method (based on Souza et al. method [15,16]), capable of applying the VCT also for unstiffened laminated composite cylindrical shells, thus nondestructively predicting their in-situ buckling loads. According to their method, a graph of $(1-p)^2$ vs. $(1-f^2)$is constructed (see Fig. 1b), based on non-dimensional values of p and f. Then a best fit second order equation is approximated based on the experimental points (Fig. 1b).

Using Fig. 1b, the fitted second order polynomic curve of the measured experimental natural frequencies would have the following expression:

$$(1-p)^2 = A\left(1-f^2\right)^2 + B\left(1-f^2\right) + C \tag{3}$$

with the values of the constants A, B and C being determined by the best fit process. Finding the minimal point of the second order equation presented in Eq. (3) yields

$$\left(1-f^2\right)_{\min} = -\frac{B}{2A} \rightarrow (1-p)^2_{\min} = C - \frac{B^2}{4A} \equiv \xi^2 \tag{4}$$

with ξ being the drop in the shell load carrying capacity, like Souza et al. [16,17] method, leading to the prediction of the in-situ tested specimen in the following form:

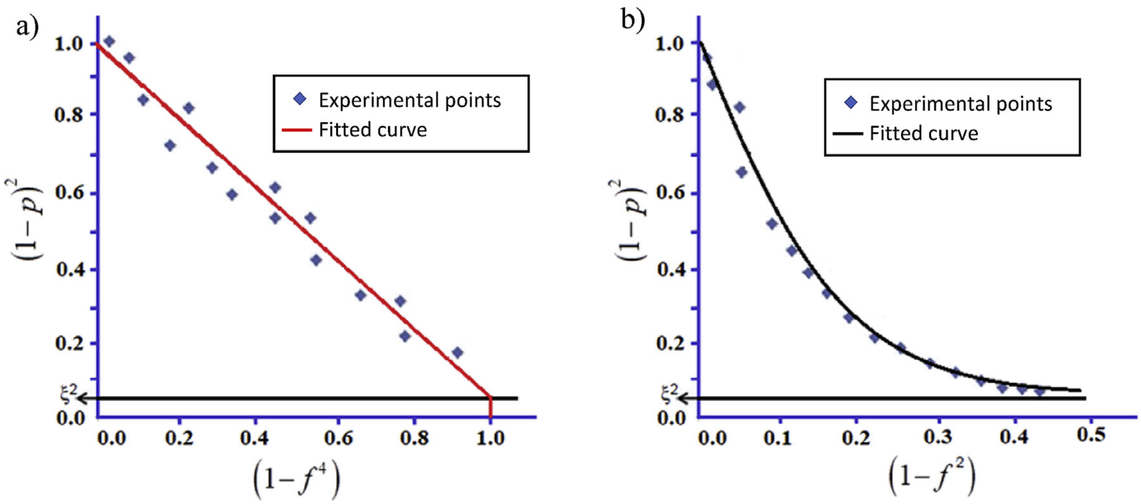

Fig. 1. Schematic determination of the predicted buckling load using VCT-a) according to Souza et al. method [15,16], b) according to Arbelo et al. method [18,19].

$$P_{pred.} = (1 - \xi)P_{cr} \tag{5}$$

3. Test specimens

Two cylindrical shells had been tested. Both have an inner diameter of 600 mm. The classical laminated shell has a length of 790 mm, while the variable angle tow composite shell has a length of 835 mm. They are composed of 8 layers of AS4/8552 Carbon Fiber Reinforced Plastic (CFRP) prepreg, each with an average thickness of 0.181 mm. Their mechanical properties are summarized in Table 1.

The layup of the classical CFRP shell is $[\pm45^\circ/0^\circ/90^\circ]_s$ which leads to a constant stiffness. The second shell is a variable angle tow CFRP shell with a layup of $[\pm45^\circ/\pm\varphi^\circ(x)]_s$, x being the shell axial coordinate, where $\pm\varphi(x)$ is a steered ply with constant route width. It has the following values: $\varphi(0) = 60^\circ$, $\varphi(L/2) = 15^\circ$ and $\varphi(L) = -60^\circ$, with L being the length of the shell. This configuration causes the shell stiffness to vary along its vertical axis.

Both cylinders have end-potting made of epoxy resin and chopped glass fibers to protect the edges of the shell from crushing during the axial compression. A plot of the two shells and a schematic drawing of the potting end-rings are presented in Fig. 2a–c.

4. Test set-up

The experimental campaign was performed at the laboratory of Aerospace Structures and Materials of the Delft University of Technology in The Netherlands. The test set-up assembly for static buckling test and VCT analysis is depicted in Fig. 3a and b. It includes a MTS 3500 kN servo-hydraulic loading rig to provide the static compressive loads and the POLYTEC PSV 500 scanning laser vibrometer. The POLYTEC set-up can measure the natural frequencies and the vibration mode shapes of the tested cylinders. It consists of a laser scanning head, data acquisition unit and a control unit, as shown in Fig. 3. The tested cylinders were excited by a loudspeaker located at the rear part of the tested specimen and controlled via an amplifier by the POLYTEC system within a predefined frequency spectrum. The measurements were conducted using a 100–400 Hz frequency sweep, the range being fixed to include most of the low natural frequencies. The laser vibrometer is capable of covering approximately 160° of the cylinder surface with high fidelity grid containing 450 points. Although to reduce the time of the scan, the scanned area was reduced to roughly 100 grid-points, without reducing the measurements accuracy. After calibration of the scanning process, a typical measurement would include the following steps: (a) the axial compressive load level is applied, (b) the loudspeaker is exciting the cylinder on a predefined frequency sweep range, while the laser scanning head is measuring the cylinder response at each predefined grid point, scanning it repeatedly five times (c), a Fast Fourie's Transform (FFT) of the cylindrical shell response presenting the natural frequencies within the predefined frequency range.

Table 1
Properties of AS4 8552 [29].

0° Tensile Strength [MPa]	2205
0° Tensile Modulus [GPa]	141
0° Tensile Strain	1.55%
0° Short Beam Shear Strength [MPa]	128
0° Compressive Strength [MPa]	1530
0° Compressive Modulus [GPa]	128

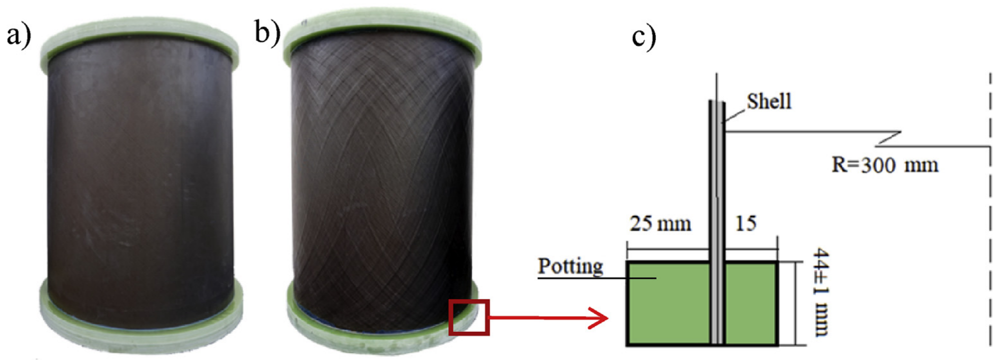

Fig. 2. Cylindrical shells: (a) Classical composite shell, (b) Variable angle tow composite shell, (c) Schematic drawing of the potting end-rings.

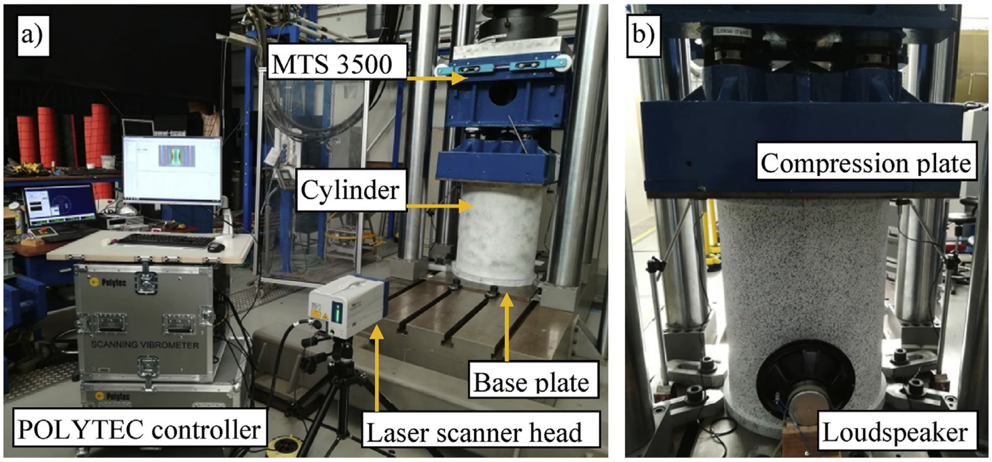

Fig. 3. The test set-up: (a) front view, (b) rear view.

The measurements, namely the natural frequencies and their associated mode shapes are saved on the POLYTEC internal storage.

5. Experimental and numerical results

The experimental campaign provided the results of static compression until the buckling as well as load-frequency responses for VCT. Numerical calculations were performed to obtain the linear and non-linear buckling loads of the tested shells, which are further used for VCT.

5.1. Static buckling of the shells

The numerical buckling analysis of both cylinders was performed using the ABAQUS 2017 finite element commercial software. The cylinders were modelled using the S4R shell-type elements with a mesh step being equal to 10 mm, while the end-potting of the shells were modelled using C3D8R element, a general purpose linear brick element with one integration point (proven to be effective in modelling of this kind of boundary conditions). The boundary conditions were set to rigidly link the nodes on the edges of the cylinder to the central reference nodes. Only a vertical displacement of the upper nodes, linked to the central node, was allowed while the lower end of the shell was restricted to move in any direction. (see Fig. 4a). The measured initial geometrical imperfection pattern applied to the shells are shown in Fig. 4b. It seems that the classical laminated shell is uniformly ovalized along its vertical axis, and the variable angle tow reinforced composite shell displays several out-of-plane areas at its bottom part The magnitude of the imperfections for the classical laminated shell lies in the range of ±1 mm and for the variable Variable angle tow shell it is in the range of $+1.5$ to -1 mm. The reference for imperfections values is the perfect cylinder shape with the radius found by best-fit method. The imperfections were included only in the non-linear numerical model yielding a reduction in the predicted buckling load, as displayed in Table 2. More information on this topic can be found in Ref. [30].

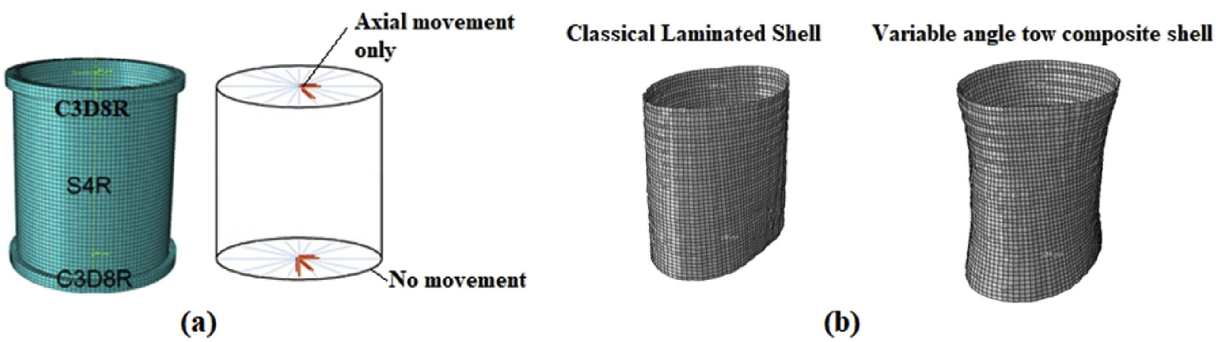

Fig. 4. (a) Mesh and boundary conditions, (b) initial geometric imperfection of the two shells magnified by a factor of 50.

Table 2
Numerical and experimental buckling loads for the two tested shells.

	Linear buckling [kN]	Non-linear buckling [kN]	Test [kN]
Classical composite shell	420	325	303
Variable angle tow composite shell	260	249	208

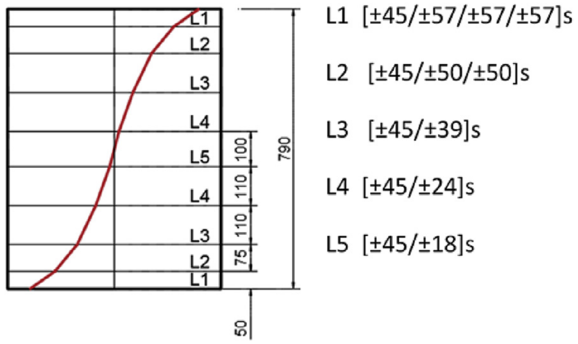

Fig. 5. Variable angle tow composite shell modelling.

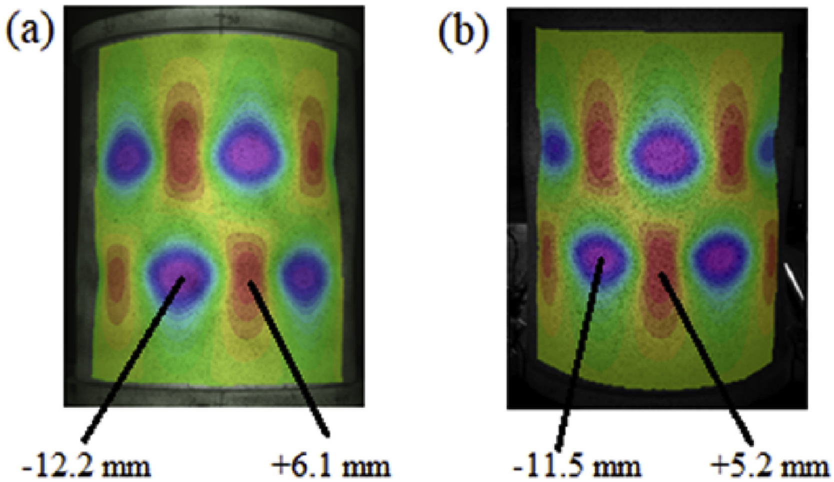

Fig. 6. Post buckling modes obtained by Digital Image Correlation System: (a) Classical laminated shell, (b) Variable angle tow composite shell.

Table 3
Experimental measured natural frequencies of the classical laminated shell.

Load [kN]	1st Frequency [Hz]	2nd Frequency [Hz]	3rd Frequency [Hz]	4th Frequency [Hz]
5	220.6	228.1	238.1	261.2
20	243.1	250.6	267.5	295.0
35	243.7	253.1	266.2	300.6
50	241.2	251.8	263.1	301.2
65	238.1	250.0	260.0	300.6
80	235.0	247.5	256.8	301.2
95	231.2	244.4	253.7	298.7
110	227.5	241.2	250.0	296.2
125	223.7	238.1	246.2	294.3
140	220.0	234.3	242.5	291.2
155	216.2	230.6	238.1	288.7
170	211.8	226.8	233.8	285.6
185	206.8	223.1	230.0	273.7
200	202.6	218.7	225.0	268.7
215	197.5	214.3	220.6	263.1
230	192.5	210.0	215.6	256.2
245	187.5	206.6	210.0	248.1
260	181.8	200.6	–	237.5
275	176.2	195.6	–	223.8

A special attention was devoted to correctly model the stiffness variation of the variable angle tow composite shell. For this purpose, the height of the shell was divided in separate sections, each with a constant layup. The ply layup for each of the sections is shown in Fig. 5. Additional plies were added for the end sections to compensate the effect of the overlapping.

The experimental buckling tests on MTS 3500 show that the classical laminated shell has a buckling load of 303 kN, with the load dropping to 75 kN, in the post buckling region, yielding two rows of buckles as shown in Fig. 6a. The second

Table 4
Experimentally measured mode shapes of the classical laminated shell.

Load [kN]	1st Frequency [Hz]	2nd Frequency [Hz]	3rd Frequency [Hz]	4th Frequency [Hz]
5	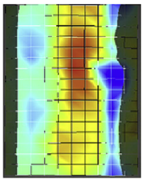	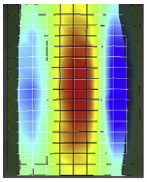	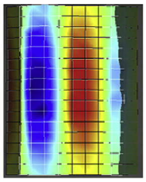	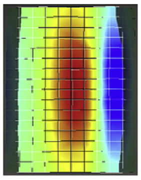
35	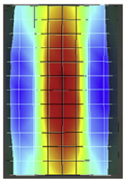	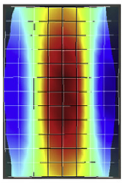	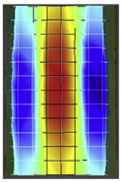	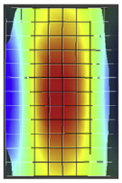
65	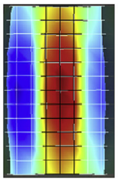	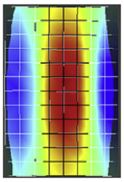	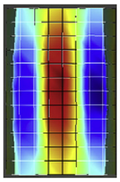	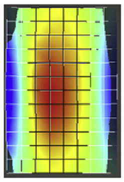
125	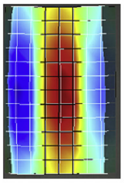	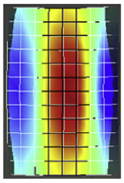	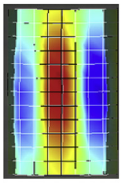	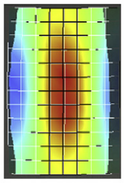
200	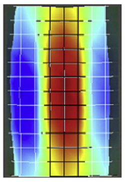	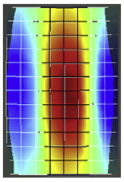	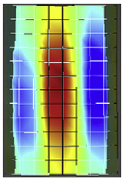	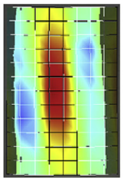
275	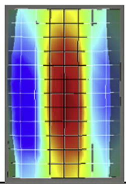	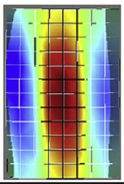	-	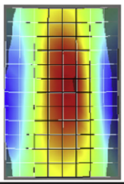
(m, n)	(14,1)	(12,1)	(14,1)	(10,1)

cylindrical shell, the variable angle tow composite shell, buckled at a lower level, 208 kN, yielding a post buckling load of 75 kN, with two rows of buckles as shown in Fig. 6b. Both shells underwent several consequent loadings and unloading cycles, with no degradation, showing a good repeatability of the buckling loads and their associated post buckling modes. Table 2 presents the various calculated buckling loads and the experimental ones. A more detailed description of the numerical modelling and experimental buckling tests is given in Ref. [30].

5.2. Excitation and measurement of natural frequencies and their associated modes

The experimental measured natural frequencies and part of the measured mode shapes are presented in Tables 3 and 4, for the classical laminate shell and in Tables 5 and 6 for the variable angle tow composite shell.

It should be noted that for both tested shells at low levels of compression loads, the natural frequencies and their associated mode shapes are not well defined, leading to natural frequencies lower than the followings ones. With the increase in the axial compression, the tested shells yielded well defined natural frequencies and mode shapes, enabling the successful application of the VCT.

Summary of the first four natural frequencies of the classical laminated cylinder is given in Table 3. The frequencies are measured with the load step of 15 kN up to the 275 kN value. By increasing the compression load level, the measured frequencies gradually decrease. Last two measurements of the 3rd frequency are invalid due to the fact that such frequency disappeared at higher load levels. The disappearing mode shapes at increasing the load level, often is the limiting factor of applying the VCT.

The mode shapes at several load steps for classical laminated shell are shown in Table 4. It can be seen that high level of noise is observable at the lowest load level. Such behavior might be explained by imperfections of the boundary conditions which disappear at higher load levels, when cylinder is loaded more uniformly. At each load level the mode shapes have a similar pattern of parallel vertical buckles, except the 4th frequency where the buckles are wider.

The numbers of circumferential and vertical half-waves (m,n) in the mode shape does not change by increasing the load, therefore they are now reported at the end of Tables 4 and 6. The number of half-waves in circumferential direction is calculated by measuring the angle of the single half-wave acquired by POLYTEC. The total number of the circumferential half-waves is the number of single waves that can fit inside 360°.

The mode shapes for the 1-3rd frequencies have a similar appearance containing 14 or 12 circumferential half-waves. The mode shapes of the 4th frequency contains only 10 circumferential half-waves.

Table 5 contains the load and natural frequency data for the variable angle tow composite shell. The load step is 10 kN to maintain the same number of data points as for the classical laminated shell. As it is expected the natural frequencies decreases by increasing the load level. The first and second natural frequencies have small differences at low load levels with almost no difference at the last load step.

Mode shapes for the variable angle tow composite shell, depicted in Table 6, maintain the same pattern at several increasing load levels. To increase the speed of VCT test, coarser mesh with only 48 grid points was used although it does not influence the results as compared to the finer mesh. The mode shapes at the forth frequency have a wider area in the middle which means that the number of buckles around the shell perimeter is lower than for the first three natural frequencies. The mode shapes at 3rd natural have a slightly non-uniform contour that could be explained by weaker response of the 3rd natural frequency comparing it to frequency 2 and 4. It could be observed in Fig. 9b. The mode shapes for the 4th frequency is

Table 5
Experimental measured natural frequencies of the variable angle tow composite shell.

Load [kN]	1st Frequency [Hz]	2nd Frequency [Hz]	3rd Frequency [Hz]	4th Frequency [Hz]
10	226.2	234.1	257.5	278.0
20	231.0	234.0	261.0	275.0
30	231.2	233.0	260.0	278.1
40	230.0	231.0	256.0	278.0
50	225.6	228.1	255.0	278.0
60	221.0	225.0	251.0	276.0
70	220.6	223.7	249.3	275.6
80	215.0	220.0	245.0	273.0
90	213.0	218.0	243.0	271.0
100	208.7	214.3	239.3	269.0
110	206.2	211.8	236.8	267.5
120	201.8	208.1	232.5	265.0
130	199.3	205.6	230.0	263.1
140	194.4	201.2	225.6	259.3
150	191.2	198.7	222.5	257.5
160	185.6	193.8	216.8	253.7
170	181.8	180.0	213.1	251.2
180	175.6	177.0	207.5	247.5

Table 6
Experimental measured mode shapes of the variable angle tow composite shell.

Load [kN]	1st Frequency [Hz]	2nd Frequency [Hz]	3rd Frequency [Hz]	4th Frequency [Hz]
10	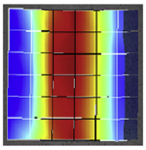	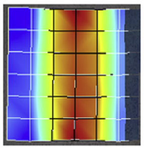	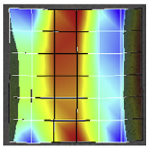	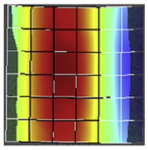
30	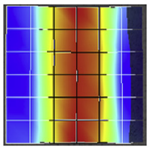	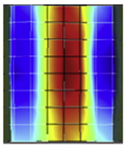	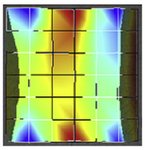	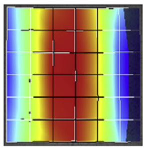
50	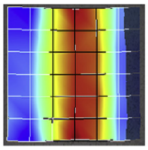	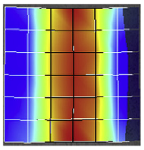	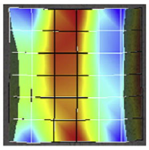	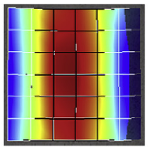
90	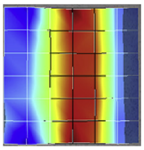	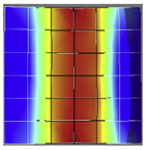	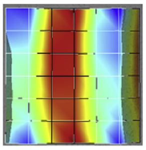	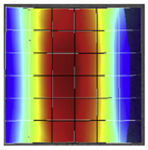
140	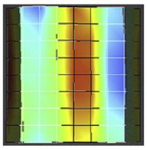	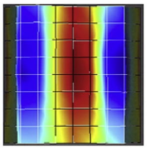	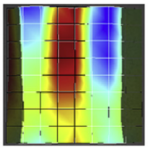	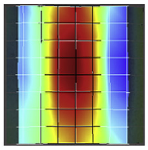
190	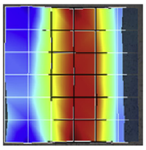	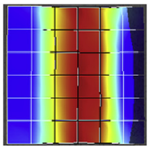	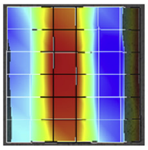	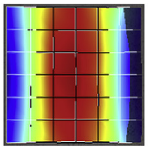
(m, n)	(12,1)	(12,1)	(14,1)	(9,1)

similar between both cylinders, containing smallest number of circumferential half-waves. First three frequencies contain mode shapes with the number of circumferential half-waves equal to 12 or 14.

To facilitate the results presented in Tables 5 and 6, Figs. 7 and 8 present a comparison between FE predictions and experimental results for the mode shapes, at two load levels for the classical and variable angle tow composite shells, respectively. Although the FE predicted frequencies are consistently higher than those experienced in the tests, the mode shapes are quite similar. The scanned area during the tests is only a smaller part of the specimen area, and therefore the single experimental half-wave mode should be compared with the frame highlighted on the FE deformation shape.

It is important to mention that, for the application of the VCT one needs only the measured values of the natural frequencies. Their associated mode shapes, also measured by the POLYTEC system, are of a secondary importance, however they allow to follow the correct path of the natural frequency reduction with the increase in the compression load.

A typical FFT output generated by the scanning POLYTEC system for the classical laminated shell at two axial compression loads, 110 kN and 170 kN is presented in Fig. 9a, while the results for the variable angle tow composite shell at are given in Fig. 9b. The various peaks presented in both figures represent the natural frequencies spectrum for the two tested shells. As can be expected, an increase in the axial compression load, move the FFT spectrum to the left side of the graph, meaning a lower stiffness being experienced by the specimen, due to its applied compressive load. Comparing the FFT spectrum of the classical laminated shell with the one belonging to the variable angle composite shell reveals that within the frequency range of 150 till 400 Hz, the classical laminated shell presents 6 well defined natural frequencies, while the second shell shows only 5 well defined peaks.

Based on the experimental data of measured loads and their associate natural frequencies, a series of curves were constructed showing the relationship between $(1\text{-}p)^2$ and $(1\text{-}f^2)$. Following Arbelo et al. [18,19]modified VCT approach, it provides a graphical representation of ξ^2 values in the generated plots. According to the procedure outlined in Section 2, the natural frequencies were normalized using the highest value of the recorded frequency, while the axial compression was normalized either by the linear buckling load or the nonlinear buckling load. Then a curve fitting procedure was applied to obtain a second order approximation equation. Finding the minimum point of the fitted curve, would provide the value of ξ^2, from which, using Eq. (5), the predicted buckling load due to the application of the VCT approach is found. Curves for first and second natural frequency of the classical laminated shell are depicted in Fig. 10, where the loads are normalized by the linear buckling load, $P_{cr\text{-}L} = 420$ kN and by the nonlinear buckling load, $P_{cr\text{-}NL} = 325$ kN (see Table 2).

Curves for the variable angle tow composite shell are presented in Fig. 11. The curves are plotted for the 1st and 2nd natural frequency where the loads are normalized by the linear buckling load, $P_{cr\text{-}L} = 260$ kN, and the nonlinear buckling load, $P_{cr\text{-}NL} = 249$ kN (Table 2). Compared to the curves presented in Fig. 10, one can notice that the data points are less uniformly distributed along the fitted curves, with points fluctuating above and below the fitted curve.

The final output of the VCT – the predicted buckling loads along with the values of the curve fitting coefficients, R^2 and ξ are summarized in Tables 7–11. The coefficient R^2 measures the global fit of the model. If $R^2 = 1$ then approximation equation has a perfect fit to the data set.

The results of the classical laminated shells applying VCT with linear buckling load are reported in Table 7 and for the results with non-linear buckling load – in Table 8.

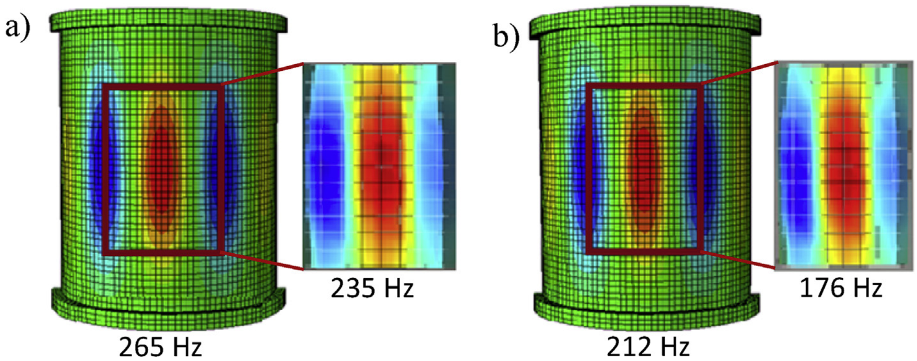

Fig. 7. The numerical and experimental vibration modes of the classical laminated shell: (a) at 80 kN load and (b) at 275 kN load.

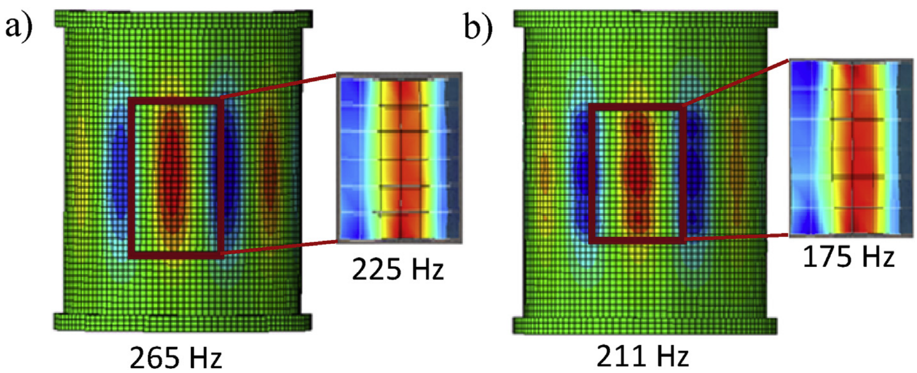

Fig. 8. The numerical and experimental vibration modes of the variable angle tow composite shell: (a) at 50 kN load and (b) at 180 kN load.

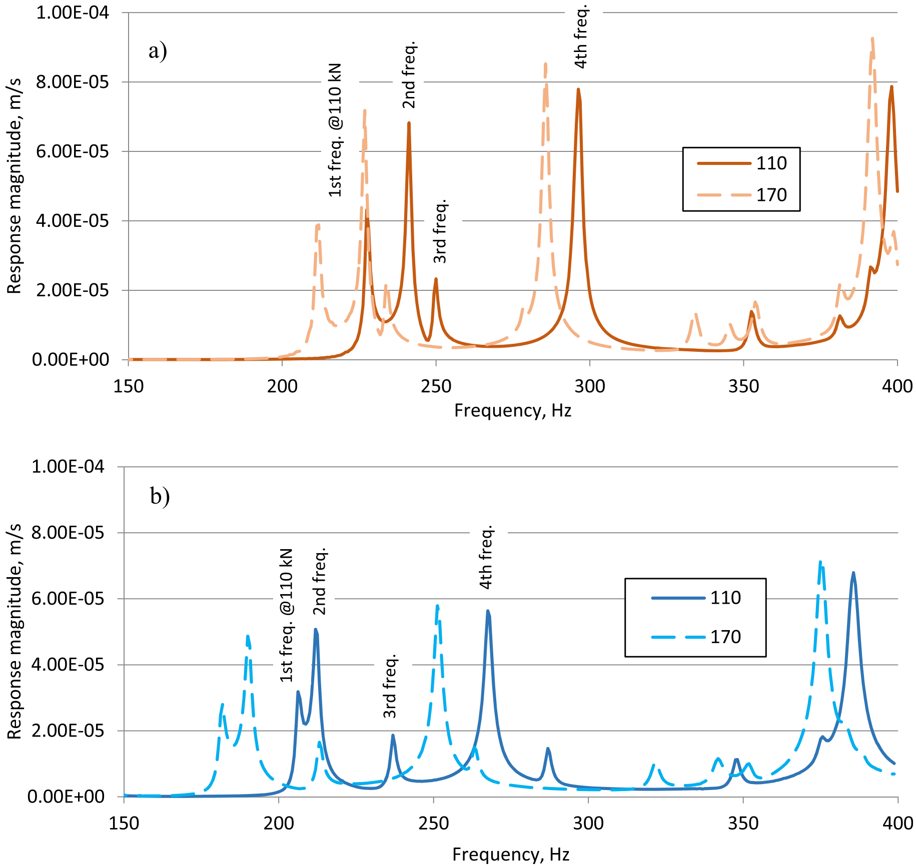

Fig. 9. FFT experimental output at two load levels: (a) Classical laminated shell, (b) Variable angle tow composite shell.

Using all the measured experimental results, would mean that the maximal normalized compression load will be $p = 275/420 = 0.65$ of the linear buckling load or $p = 275/325 = 0.85$ of the calculated nonlinear load. From engineering considerations, about 65% of the calculated buckling loads, would be a safe margin to prevent unexpected premature experimental buckling of the specimens. It was also tried to obtain P_{pred} by smaller number of the data points, based on experimental loads up to 245 kN for the linear case (yielding $p = 0.58$) or up to 200 kN for the nonlinear case (obtaining $p = 0.61$). These results were added in the end of each table for the first frequency. Undersampling in the current work is performed by reducing the number of the data points used to calculate the buckling load according to VCT by a number of 2 (from 18). The data points close to actual buckling are the most significant in determining the accurate buckling load by VCT, especially in the presence of high scatter of measured frequency responses, as in the case of the variable angle tow composite shell.

Next the output for the variable angle tow composite shell is presented in Tables 9 and 10. Like for the previous shell, also here the results are presented for VCT with linear load (Table 9) and non-linear load (Table 10). Using all the data points means that maximal p ratio will be 0.69 for linear and 0.72 for non-linear load. The results shows that the most accurate VCT predictions are obtained using the first natural frequency. The following frequencies under-predict the experimental buckling load (208 kN) by 10–13%. Considering that numerically calculated linear and non-linear buckling load for this cylinder is close, there is only minor difference between VCT results in Tables 9 and 10.

Also smaller data sets were examined to check the accuracy of VCT at lower load levels. These results, added in the last row of Tables 9 and 10, show the values which slightly exceed the experimental ones.

The summary of all the VCT results, normalized by the experimental buckling load values of 303 kN for the classical laminated shell and 208 kN for the variable angle tow composite shell (as already presented in section 5.1), is given in Table 11. One should note that the normalized results using the ρ letter is common for describing the stability of thin walled shells, usually displaying the ratio of the experimental buckling load (the numerator) to the numerical buckling load (at the denominator). The predicted buckling results using the VCT approach are based on all the experimental points, except the lines with $_{(\text{reduced\_p})}$ subscript.

Analyzing the results in Table 11, it is clearly seen that the best buckling prediction in comparison with the actual experimental one, is provided by the VCT approach using the 1st natural frequency and linear calculated buckling load. It

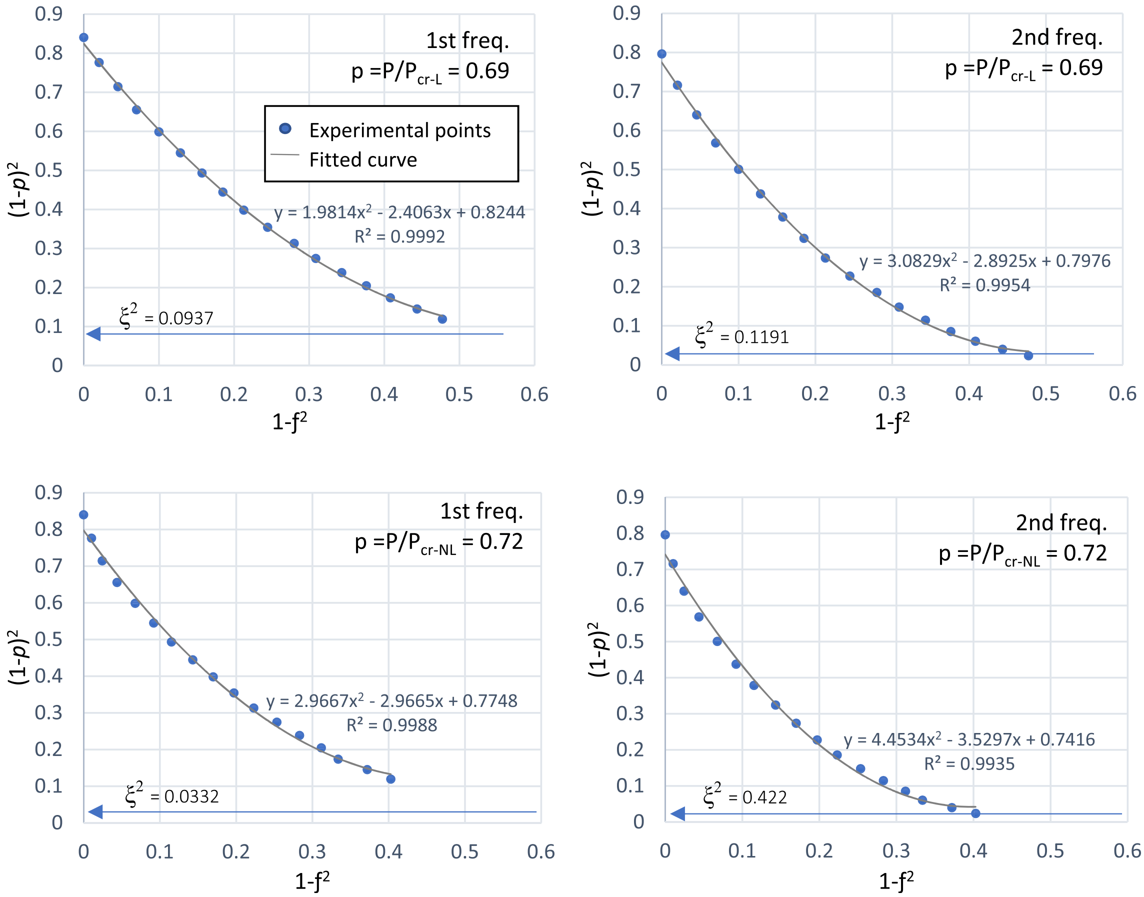

Fig. 10. Classical laminated shell- Experimental points and curve fitting.

yields values of $(\rho_{f1})_L = 0.96$ for the classical laminated shell and $(\rho_{f1})_L = 0.986$ for the variable angle tow composite shell. Prediction of the buckling load, using higher natural frequencies data reduces the effectiveness of the VCT method, thus obtaining less accurate buckling loads. Also, as depicted in Table 11, row 4 for the classical laminated shell reducing the number of experimental points for the prediction of the buckling load using VCT, leads to values smaller than the actual experimental buckling loads. For the variable angle tow composite shell, it leads to values higher than the actual experimental buckling load, diminishing the nondestructive characteristics of the VCT approach.

6. Conclusions

Two laminated composite shells, one having a classical laminate and the second one with a variable angle tow along its length, have been excited and their natural frequencies and mode shapes have been measured and monitored as a function of the applied axial compression load. Using the measured natural frequencies, the in-situ buckling loads of the two tested shells were predicted using the VCT and compared with the actual experimental buckling loads and the FE buckling predictions, yielding consistent results. Based on the present experimental campaign, the following conclusions can be drawn:

a. The application of the VCT yielded accurate predictions of the actual experimental buckling loads of the two tested shells, acceptable from the engineering point of view. Using the linear buckling load and lowest natural frequency, the method under predicted the buckling load by only 4% for the case of classical laminated shell and 1.4% for the variable angle tow composite shell. Using the other measured natural frequencies to predict the buckling load still exhibited under prediction of the buckling loads, with less accurate values.
b. Changing the normalizing load to the nonlinear buckling load or reducing the number of experimental points leads to worst predictions, and therefore it is recommended to choose the linear value as the reference. Yet it should be stressed that this recommendation is based on the present experimental results and more tests should be performed for its full validation.

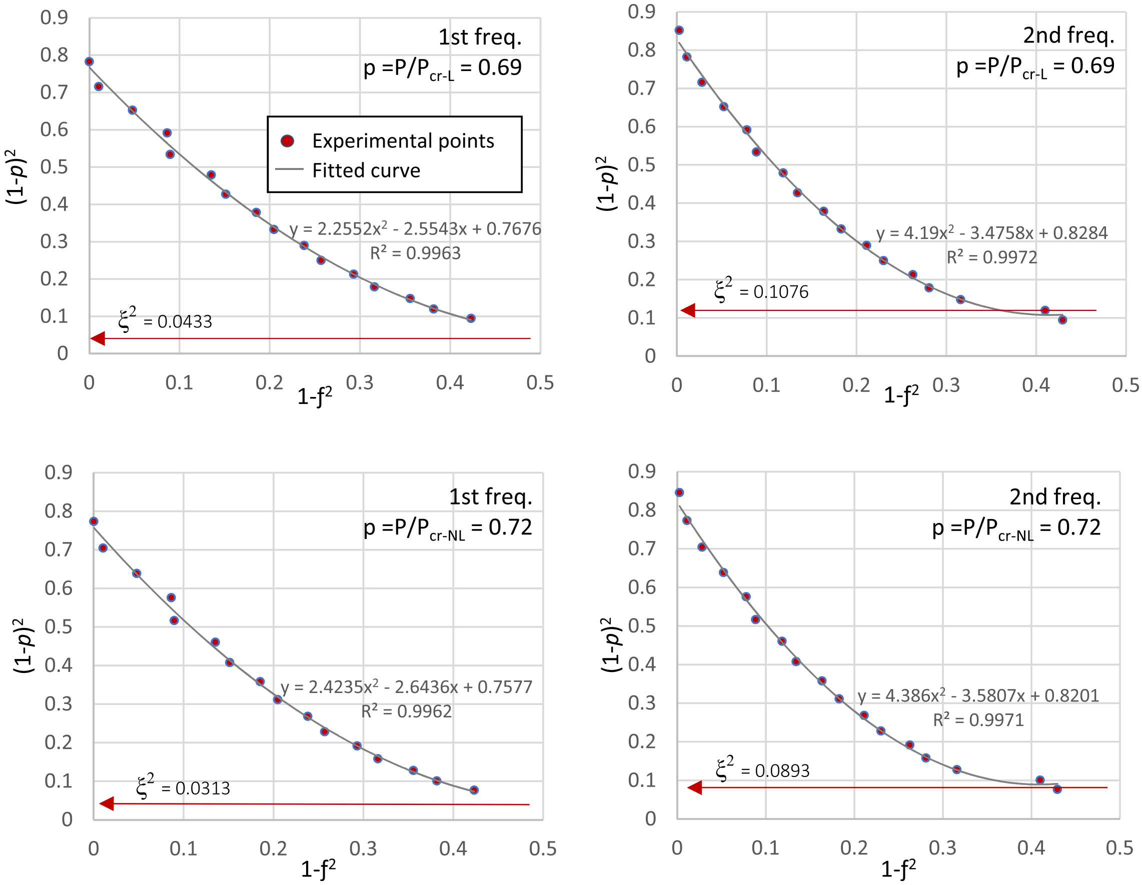

Fig. 11. Variable Angle Tow Composite Shell- Experimental points and curve fitting.

Table 7
Classical laminated shell-loads normalized by $P_{cr\text{-}L} = 420$ [kN].

Freq. No.	Up to $p =$	Coefficients of the fitted curves			[R^2]	ξ	$P_{pred.}$ [kN]
		A	B	C			
1st	0.65	1.9814	−2.4063	0.8244	0.9992	0.306	291
2nd	0.65	3.0829	−2.8925	0.7976	0.9954	0.345	275
3rd	0.65	2.7166	−2.9200	0.9296	0.9996	0.381	260
4th	0.65	2.7700	−2.2886	0.6095	0.9736	0.370	265
1st	0.58	2.1653	−2.4688	0.8272	0.9993	0.351	272

Table 8
Classical laminated shell-loads normalized by $P_{cr\text{-}NL} = 325$ [kN].

Freq. No.	Up to $p =$	Coefficients of the fitted curves			[R^2]	ξ	$P_{pred.}$ [kN]
		A	B	C			
1st	0.85	2.9667	−2.9665	0.7748	0.9988	0.182	266
2nd	0.85	4.4534	−3.5297	0.7416	0.9935	0.205	258
3rd	0.85	4.4126	−3.6950	0.8418	.9973	0.261	240
4th	0.85	3.4425	−2.5658	0.5108	0.9641	0.181	266
1st	0.615	3.7225	−3.1903	0.7838	0.9992	0.317	222

c. The lack of the capability to measure the mode shapes, should not prevent the application of the described non-destructive method. The measured mode shapes serve only to monitor the correct path of the experimental natural frequencies that decreases as a function of the compression load increase.

Table 9
Variable angle tow composite shell-loads normalized by $P_{cr} = 260$ [kN].

Freq. No.	Up to $p =$	Coefficients of the fitted curves			[R^2]	ξ	$P_{pred.}$ kN]
		A	B	C			
1st	0.69	2.2552	−2.5543	0.7676	0.9963	0.2106	205
2nd	0.69	4.1900	−3.4758	0.8284	0.9972	0.328	175
3rd	0.69	3.8374	−3.3588	0.8137	0.9979	0.281	187
4th	0.69	10.618	−4.7784	0.6396	0.9956	0.319	177
1st	0.615	2.1562	−2.5248	0.7664	0.9951	0.165	217

Table 10
Variable angle tow composite shell-loads normalized by $P_{cr\text{-}NL} = 249$ [kN].

Freq. No.	Up to $p =$	Coefficients of the fitted curves			[R^2]	ξ	$P_{pred.}$ [kN]
		A	B	C			
1st	0.72	2.4235	−2.6436	0.7577	0.9962	0.177	205
2nd	0.72	4.386	−3.5807	0.8201	0.9971	0.299	176
3rd	0.72	4.086	−3.4745	0.8054	0.9978	0.258	185
4th	0.72	11.167	−4.906	0.6252	0.9954	0.294	176
1st	0.64	2.333	2.6167	0.7567	0.9950	0.152	211

Table 11
Summary of the results.

Non-dimensional Load[a]	Classical Laminated Shell	Variable Angle Tow Composite Shell
Calculated Linear - ρ_L	1.386	1.250
Calculated Nonlinear- ρ_{NL}	1.073	1.197
VCT predicted- $(\rho_{f1})_L$	*0.960*	*0.986*
VCT predicted- $(\rho_{f1})_{L(reduced\_p)}$	0.898	1.043
VCT predicted- $(\rho_{f2})_L$	0.908	0.841
VCT predicted- $(\rho_{f3})_L$	0.858	0.899
VCT predicted- $(\rho_{f4})_L$	0.875	0.851
VCT predicted- $(\rho_{f1})_{NL}$	0.878	0.986
VCT predicted- $(\rho_{f1})_{NL(reduced\_p)}$	0.733	1.014
VCT predicted- $(\rho_{f2})_{NL}$	0.851	0.846
VCT predicted- $(\rho_{f3})_{NL}$	0.792	0.889
VCT predicted- $(\rho_{f4})_{NL}$	0.878	0.846

[a] $(\rho_{f(i)})_L$ and $(\rho_{f(i)})_{NL}$ are the VCT predicted buckling loads, divided by the experimental buckling loads, based on 1st, 2nd, 3rd and 4th measured natural frequency, where the axial compression is normalized by the linear or nonlinear buckling loads, respectively.

d. Using a loudspeaker as a means to excite the tested shell, proved to be a reliable source of excitation (although located outside the specimen) yielding consistent and repeatable results.
e. The VCT proved to be an adequate nondestructive method to assess the actual in-situ buckling load, of laminated composite thin walled cylindrical shells with a high accuracy.
f. Based on the present and previous studies, it is recommended to have at least 15 experimental point to reach a reliable buckling prediction, using the VCT.
g. For cases where the lowest natural frequency cannot be detected, and the prediction is done using the second lowest frequency, the buckling prediction will be less accurate (90% of the experimental buckling load, compared to 96% when using the lowest natural frequency), however the nondestructive nature of the VCT is preserved.

References

[1] M.P. Nemeth, J.H. Starnes, The NASA Monographs on Shell Stability Design Recommendations, NASA/TP-1998-206290, 1998, pp. 1–20. https://ntrs.nasa.gov/archive/nasa/casi.ntrs.nasa.gov/19980147983.pdf. (Accessed 13 June 2018).
[2] V.I. Weingarten, P. Seide, P. Peterson, Buckling of Thin-Walled Circular Cylinders, NASA SP-8007, 1968, pp. 1–60. https://ntrs.nasa.gov/archive/nasa/casi.ntrs.nasa.gov/19690013955.pdf. (Accessed 13 June 2018).
[3] V.I. Weingarten, P. Seide, Buckling of Thin-Walled Doubly Curved Shells, NASA SP-8032, 1969, pp. 1–37. https://www.scribd.com/document/369438426/NASA-sp8032-Space-Vehicle-Design-Criteria-Buckling-of-Thin-Walled-Double-Curved-Shells-pdf. (Accessed 13 June 2018).
[4] M.W. Hilburger, Developing the next generation shell buckling design factors and technologies, in: 53rd AIAA/ASME/ASCE/AHS/ASC Struct. Struct. Dyn. Mater. Conf., Honolulu, Hawaii, 2012, pp. 1–15, https://doi.org/10.2514/6.2012-1686.
[5] C. Bisagni, Overview of the DAEDALOS project, Prog. Aero. Sci. 78 (2015) 1–7, https://doi.org/10.1016/J.PAEROSCI.2015.05.007.
[6] C. Bisagni, Composite cylindrical shells under static and dynamic axial loading: an experimental campaign, Prog. Aero. Sci. 78 (2015) 107–115, https://doi.org/10.1016/J.PAEROSCI.2015.06.004.

[7] H. Abramovich, C. Bisagni, Behavior of curved laminated composite panels and shells under axial compression, Prog. Aero. Sci. 78 (2015) 74–106, https://doi.org/10.1016/J.PAEROSCI.2015.05.008.
[8] S.G.P. Castro, R. Zimmermann, M.A. Arbelo, R. Khakimova, M.W. Hilburger, R. Degenhardt, Geometric imperfections and lower-bound methods used to calculate knock-down factors for axially compressed composite cylindrical shells, Thin-Walled Struct. 74 (2014) 118–132, https://doi.org/10.1016/J.TWS.2013.08.011.
[9] J. Singer, J. Arbocz, T. Weller, Buckling Experiments: Experimental Methods in Buckling of Thin-Walled Structures, John Wiley & Sons, Inc., Hoboken, NJ, USA, 2002, https://doi.org/10.1002/9780470172995.
[10] H. Abramovich, Stability and Vibrations of Thin-Walled Composite Structures, first ed., Woodhead Publishing, UK, 2017.
[11] J. Singer, H. Abramovich, Vibration techniques for definition of practical boundary conditions in stiffened shells, AIAA J. 17 (1979) 762–769, https://doi.org/10.2514/3.61215.
[12] A. Rosen, J. Singer, Effect of axisymmetric imperfections on the vibrations of cylindrical shells under axial compression, AIAA J. 12 (1974) 995–999, https://doi.org/10.2514/3.49393.
[13] J. Singer, J. Prucz, Influence of initial geometrical imperfections on vibrations of axially compressed stiffened cylindrical shells, J. Sound Vib. 80 (1982) 117–143, https://doi.org/10.1016/0022-460X(82)90396-0.
[14] H. Abramovich, D. Govich, A. Grunwald, Buckling prediction of panels using the vibration correlation technique, Prog. Aero. Sci. 78 (2015) 62–73, https://doi.org/10.1016/J.PAEROSCI.2015.05.010.
[15] M.A. Souza, W.C. Fok, A.C. Walker, Review of experimental techniques for thin-walled structures liable to buckling Part I-neutral and unstable buckling, Exp. Tech. 7 (1983) 21–25. https://onlinelibrary.wiley.com/doi/pdf/10.1111/j.1747-1567.1983.tb01811.x. (Accessed 13 June 2018).
[16] M.A. Souza, L.M.B. Assaid, A new technique for the prediction of buckling loads from nondestructive vibration tests, Exp. Mech. 31 (1991) 93–97, https://doi.org/10.1007/BF02327558.
[17] E.L. Jansen, H. Abramovich, R. Rolfes, The direct prediction of buckling loads of shells under axial compression using VCT -Towards an upgraded approach, in: Proc. ICAS 2014, 29th Congr. Int. Counc. Aeronaut. Sci., St. Petersburg, Russia, 2014, pp. 1–9. http://www.icas.org/ICAS_ARCHIVE/ICAS2014/data/papers/2014_0681_paper.pdf. (Accessed 13 June 2018).
[18] M.A. Arbelo, S.F.M. de Almeida, M.V. Donadon, S.R. Rett, R. Degenhardt, S.G.P. Castro, K. Kalnins, O. Ozoliņš, Vibration correlation technique for the estimation of real boundary conditions and buckling load of unstiffened plates and cylindrical shells, Thin-Walled Struct. 79 (2014) 119–128, https://doi.org/10.1016/J.TWS.2014.02.006.
[19] M.A. Arbelo, K. Kalnins, O. Ozolins, E. Skukis, S.G.P. Castro, R. Degenhardt, Experimental and numerical estimation of buckling load on unstiffened cylindrical shells using a vibration correlation technique, Thin-Walled Struct. 94 (2015) 273–279, https://doi.org/10.1016/J.TWS.2015.04.024.
[20] E. Skukis, O. Ozolins, K. Kalnins, M.A. Arbelo, Experimental test for estimation of buckling load on unstiffened cylindrical shells by vibration correlation technique, Procedia Eng. 172 (2017) 1023–1030, https://doi.org/10.1016/J.PROENG.2017.02.154.
[21] K. Kalnins, M.A. Arbelo, O. Ozolins, E. Skukis, S.G.P. Castro, R. Degenhardt, Experimental nondestructive test for estimation of buckling load on unstiffened cylindrical shells using vibration correlation technique, Shock Vib. (2015) 1–8, https://doi.org/10.1155/2015/729684. ID 729684.
[22] E. Skukis, O. Ozolins, J. Andersons, K. Kalnins, M.A. Arbelo, Applicability of the vibration correlation technique for estimation of the buckling load in axial compression of cylindrical isotropic shells with and without circular cutouts, Shock Vib. (2017) 1–14, https://doi.org/10.1155/2017/2983747. ID 2983747.
[23] Z. Gürdal, B.F. Tatting, C.K. Wu, Variable stiffness composite panels: effects of stiffness variation on the in-plane and buckling response, Compos. Part A Appl. Sci. Manuf. 39 (2008) 911–922, https://doi.org/10.1016/J.COMPOSITESA.2007.11.015.
[24] G. Raju, Z. Wu, B.C. Kim, P.M. Weaver, Prebuckling and buckling analysis of variable angle tow plates with general boundary conditions, Compos. Struct. 94 (2012) 2961–2970, https://doi.org/10.1016/J.COMPSTRUCT.2012.04.002.
[25] Z. Wu, G. Raju, P.M. Weaver, Postbuckling analysis of variable angle tow composite plates, Int. J. Solids Struct. 50 (2013) 1770–1780, https://doi.org/10.1016/J.IJSOLSTR.2013.02.001.
[26] Z. Wu, G. Raju, P.M. Weaver, Framework for the buckling optimization of variable-angle tow composite plates, AIAA J. 53 (2015) 3788–3804, https://doi.org/10.2514/1.J054029.
[27] P.M. Weaver, Z.M. Wu, G. Raju, Optimisation of variable stiffness plates, Appl. Mech. Mater. 828 (2016) 27–48, https://doi.org/10.4028/www.scientific.net/AMM.828.27.
[28] S.C. White, P.M. Weaver, Towards imperfection insensitive buckling response of shell structures-shells with plate-like post-buckled responses, Aeronaut. J. 120 (2016) 233–253, https://doi.org/10.1017/aer.2015.14.
[29] HexTow Laminate Properties in HexPly 8552, (n.d.). http://www.hexcel.com/Products/Resources/1664/hextow-laminate-properties-in-hexply-8552.
[30] E. Labans, C. Bisagni, Buckling and free vibration study of variable and constant-stiffness cylindrical shells, Compos. Struct. 210 (2019) 446–457, https://doi.org/10.1016/j.compstruct.2018.11.061.